SAND2021-10362J

A Forward Analytic Model of Neutron Time-of-Flight Signals for Inferring Ion Temperatures from MagLIF Experiments

Colin Weaver,*,[a] Gary Cooper,[a] Christopher Perfetti,[a] David Ampleford,[b] Gordon Chandler,[b] Patrick Knapp,[b] Michael Mangan,[b] and Jedediah Styron[a]

[a] *University of New Mexico, Department of Nuclear Engineering*

[b] *Sandia National Laboratories, Fusion Experiments Department*

*Email: caweave@sandia.gov

Number of pages: 34
Number of tables: 6
Number of figures: 9

Sandia National Laboratories is a multimission laboratory managed and operated by National Technology & Engineering Solutions of Sandia, LLC, a wholly owned subsidiary of Honeywell International Inc., for the U.S. Department of Energy's National Nuclear Security Administration under contract DE-NA0003525.

Abstract

A forward analytic model is required to rapidly simulate the neutron time-of-flight (nToF) signals that result from magnetized liner inertial fusion (MagLIF) experiments at Sandia's Z Pulsed Power Facility. Various experimental parameters, such as the burn-weighted fuel-ion temperature and liner areal density, determine the shape of the nToF signal and are important for characterizing any given MagLIF experiment. Extracting these parameters from measured nToF signals requires an appropriate analytic model that includes the primary DD neutron peak, once-scattered neutrons in the beryllium liner of the MagLIF target, and direct beamline attenuation. Mathematical expressions for this model were derived from the general-geometry time- and energy-dependent neutron transport equation with anisotropic scattering. Assumptions consistent with the time-of-flight technique were used to simplify this linear Boltzmann transport equation into a more tractable form. Models of the un-collided and once-collided neutron scalar fluxes were developed for one of the five nToF detector locations at the Z Machine. Numerical results from these models were produced for a representative MagLIF problem and found to be in good agreement with similar neutron transport simulations. Twenty experimental MagLIF data sets were analyzed using the forward models, which were determined to only be significantly sensitive to the ion temperature. The results of this work were also found to agree with values obtained separately using a zero scatter analytic model and a high fidelity Monte Carlo simulation. Inherent difficulties in this and similar techniques are identified, and a new approach forward is suggested.

Keywords — Z Pulsed Power Facility, Magnetized Liner Inertial Fusion, Neutron Time-of-Flight

I. INTRODUCTION

Sandia National Laboratories' Z Pulsed Power Facility is the largest pulsed power facility in the world. It is used for a wide variety of research that is intended, in part, to increase our understanding of basic fusion science and technology. Pulsed power has proven to be an important tool for studying high energy density physics such as dynamic material properties, radiation science, and inertial confinement fusion (ICF) [1]. Z is one of three flagship facilities in the U.S. Inertial Confinement Fusion Program, and is the primary facility for magnetic direct drive fusion [2].

The goal of this work is to develop a model that reproduces neutron time-of-flight (nToF) signals given a set of uncertain plasma conditions from ICF experiments conducted at the Z Pulsed Power Facility. This new model will be an analytic function of the nToF detector's time-space as well as several experimental parameters of interest that are important for characterizing an ICF experiment, e.g., the burn-weighted ion temperature, the liner areal density, and the neutron-burn time history. Some of these parameters are extracted from experimental nToF data by using this model in conjunction with a nonlinear least-squares fitting routine.

II. MAGNETIZED LINER INERTIAL FUSION

Pulsed power compresses electrical energy in space and time to produce short bursts of high power which generate high energy density conditions [3]. The Z-machine can convert 22 MJ of energy stored in 36 Marx generators to 3 MJ of energy deliverable to the center section load hardware in the form of $\sim$100 Mbar drive pressures and $\sim$26 MA currents [2]. These conditions allow the Z-Machine to produce $>$1 MJ of x-rays, which also makes it the most powerful x-ray source in the world [4, 5, 6].

The Sandia Inertial Confinement Fusion program is interested in magnetic direct drive target research [7], which utilizes the J$\times$B force that results from a massive electric current flowing through a small magnetized target [8]. One effort in this campaign is Magnetized Liner Inertial Fusion (MagLIF) [9, 10], a magneto-inertial fusion concept [11]. It relies on three components to produce fusion conditions at stagnation: magnetization, laser preheat, and magnetically driven implosion [8, 12, 13, 14].

The magnetization step of the process imposes a 10-30 T axial magnetic field on a cylindrical

beryllium liner filled with D_2 gas [12]. This is followed by a 100-200 eV laser preheat from the Z-Beamlet Laser [15]. Finally, ∼20 MA of current is driven through the cylinder and J×B forces compress the liner at ∼100 km/s. In this process the pre-imposed B-field is amplified to >10,000 T and PdV work heats the fuel creating a short lived, neutron producing, plasma.

The primary nuclear reaction in a MagLIF experiment is the deuterium-deuterium (DD) fusion reaction. DD fusion reactions produce 2.45 MeV neutrons on average. Their detection in a MagLIF experiment indicates that nuclear fusion has occurred [13], which is important for characterizing MagLIF experiments in terms of plasma parameters such as the ion temperature.

The energy distribution of DD neutrons emanating from a MagLIF target is described analytically by a modified Gaussian function

$$I(E) = I_0 \exp\left(-\frac{2\bar{E}}{\sigma^2}\left(\sqrt{E} - \sqrt{\bar{E}}\right)^2\right), \tag{1}$$

where I_0 is a normalization factor, and the parameters $\bar{E}$ and σ are dependent on the ion temperature of the plasma. Details of this dependency can be found in [16]. To take advantage of the fact that neutron measurements can be used to infer plasma ion temperatures, five neutron time-of-flight detector locations were placed around Z. Each detector is located in one of three lines-of-sight (LOS) and are situated at various distances from the center section of Z. A collimator and vacuum section in the LOS filter the neutrons so that only those traveling toward the detector are allowed through the LOS. To produce a clean neutron signal, high-Z attenuators are also placed along the LOS to limit the number of photons reaching the detector.

In addition to DD neutrons, subsequent neutrons produced from deuterium-tritium (DT) reactions, x-rays, and bremsstrahlung radiation are also emitted from the target. In order to broaden the nToF signal in time and spread out the individual components of the signal due to various particles of different energies, the nToF detectors are placed 7 m, 8 m, 9.5 m, 11.5 m, and 25 m away from the target. The 9.5 m and 11.5 m nToF detectors are located in the same line-of-sight (LOS 270), but only the front 9.5 m nToF detector will be considered in this work. A description of LOS 270 can be found in Subsection IV.A.3.

Figure 1 illustrates a typical nToF signal from the front LOS 270 detector. In general, a nToF signal at Z is characterized by five distinct regions that correspond to particles arriving at the detector in order of their relative velocities. The fastest particles are photons, which make

up the x-ray and bremsstrahlung component of the signal. This is followed by the secondary 14.1 MeV DT neutron peak and its subsequent downscatter region, which are barely visible in this picture. The primary 2.45 MeV DD neutron peak and the beryllium liner downscatter region comes next. They are arguably the most important regions of the nToF signal, because that is where parameters of a MagLIF experiment can be inferred. Finally, neutrons emanating from the target can scatter throughout Z and travel toward any of the detectors. However, the component of the signal due to these interactions is usually insignificant.

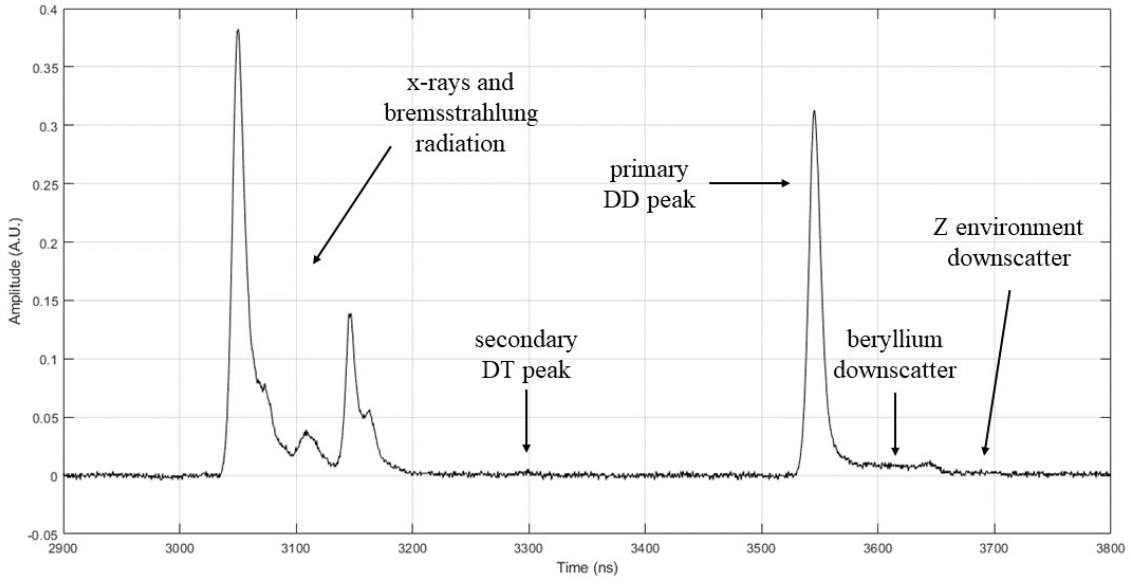

Fig. 1. A typical nToF signal from the front LOS 270 detector.

III. METHODOLOGY

Pre-implosion MagLIF target specifications are known prior to each experiment. However, the resulting plasma and liner conditions are unknown at the stagnation point. The physical dimensions and density of the liner vary for each implosion at bang-time, and the ion temperature, density, and time history of the plasma are always different. This work demonstrates how the ion temperature can be inferred from MagLIF nToF signals.

The general approach to tackling this problem is to propose a model that captures the relevant physics of a MagLIF experiment and fit it to experimental nToF data. The nToF signal is a convolution of several time-dependent quantities. One of these quantities is the instrument

response function (IRF) which is purely a function of the detector properties. Hence, it would be beneficial to unfold the IRF from the nToF signal since it does not contain any information on the implosion conditions. Unfortunately, this type of mathematical problem is generally ill-posed, and unique deconvolution solutions are not expected to exist [17]. Thus, the traditional course of action is to convolve the IRF with a forward neutron spectrum model and fit the resulting objective function to experimental data using a nonlinear least-squares algorithm. Similar techniques can be found in literature [18, 19].

The two main approaches to modeling the neutron spectrum arriving at a nToF detector are to develop an analytic model from first principles and to simulate particles moving through the system using a neutron transport code. The method developed in this work falls under the first category. However, the results of two separate methods from each approach have been used in the past, and their results are included later as a comparison for this work. The goal of this work is to develop a model that reproduces nToF signals given a set of uncertain MagLIF plasma conditions. We propose a neutron spectrum model that is analytically determined and captures the relevant physics of neutron scattering and attenuation in LOS 270. This is a solution that should produce more accurate ion temperature measurements than a zero scatter analytic model and at the same time will be faster than Monte Carlo (MC) simulations.

For the sake of informing an appropriate analytic model with scattering, neutron interactions in the fuel and liner should be considered heuristically at first. This is done by investigating the microscopic cross-sections of deuterium and beryllium, as well as their angular distributions for elastically scattered neutrons. The ENDF database [20] shows the microscopic cross-sections of deuterium for elastic and non-elastic scattering events. The primary DD neutrons, with neutron energies between 2-3 MeV, are only likely to undergo elastic scattering reactions as they exit the target. Forward scattering is preferential in the fuel region of the target. Hence, neutrons exiting the plasma after a scattering collision are likely to remain near their initial energies. This coupled with the fact that the neutron mean free path is much longer than the plasma size indicates that the contribution to the nToF signal from elastic scattering in the fuel is small.

The microscopic cross-sections of Be-9 for elastic and non-elastic scattering events show that neutron interactions in the energy range 2-3 MeV are dominated by elastic scattering with some $(n, 2n)$ reactions. In contrast to deuterium, scattering off of Be-9 nuclei generally produce bimodal

energy distributions. Hence, neutrons exiting the liner after an elastic scattering collision are more likely to be at the tail ends of the scattering energy interval. This coupled with the fact that the neutron mean free path is shorter than the liner size indicates that the contribution to the nToF signal from elastic scattering in the liner is large.

These heuristic arguments indicate that an analytic model of the neutron spectrum should include at least: the primary DD neutron peak, single elastic scattering in the beryllium liner, and attenuation through the line-of-sight.

IV. THE NEUTRON TIME-OF-FLIGHT SIGNAL

The nToF signal describes the number of neutrons arriving at a nToF detector as a function of time. It is represented mathematically as the convolution of several time-dependent quantities

$$S(t) = [N \otimes T \otimes R](t). \tag{2}$$

Here, $S(t)$ is the detector signal, $N(t)$ is the neutron spectrum, $T(t)$ is the neutron-burn time history, and $R(t)$ is the instrument response function.

The three functions on the right-hand-side of (2) form the basis for a forward model of a measured nToF signal. They are parameterized in terms of important physical quantities that can be extracted from experimental data using nonlinear least-squares fitting routines or a Bayesian inference formalism. The inherent difficulty of such a problem is determining appropriate expressions for $N(t)$, $T(t)$, and $R(t)$ that are conducive for an iterative solver to converge on solutions in a unique and timely manner while also accurately describing the physics.

IV.A. The Neutron Spectrum

The neutron spectrum describes the number of neutrons arriving at a nToF detector in some time interval of interest. It is the most important component of the nToF signal, because it is where the physical parameters of the source plasma can be inferred. In particular, the ion temperature and liner areal density can be extracted from the primary DD signal and beryllium liner down-scatter region. Determining this expression requires knowing how neutrons will travel through the MagLIF experimental setup.

Neutrons propagate through a system according to a linear Boltzmann transport equation. For a MagLIF experiment, the particular transport equation is 3D time- and energy-dependent with anisotropic scattering. In general, analytic solutions do not exist for this type of neutron transport equation. However, appropriate assumptions that are consistent with the time-of-flight method can be used to simplify the equation into a more tractable form.

IV.A.1. The Neutron Transport Equation

The general-geometry time- and energy-dependent neutron transport equation with a fixed source is given by [21, 22, 23]

$$\frac{1}{v}\frac{\partial}{\partial t}\psi\left(\vec{r},E,\vec{\Omega},t\right)+\vec{\Omega}\cdot\nabla\psi\left(\vec{r},E,\vec{\Omega},t\right)+\Sigma_t\left(\vec{r},E\right)\psi\left(\vec{r},E,\vec{\Omega},t\right)$$
$$=\int_0^\infty dE'\int_{4\pi}d\vec{\Omega}'\;\Sigma_s\left(\vec{r},E'\rightarrow E,\vec{\Omega}'\rightarrow\vec{\Omega}\right)\psi\left(\vec{r},E',\vec{\Omega}',t\right)+Q\left(\vec{r},E,\vec{\Omega},t\right), \quad (3)$$

where ψ is the neutron angular flux, $\vec{r}$ is the neutron's position in space, $v(E)$ is the neutron's energy dependent velocity, $\vec{\Omega}$ is the neutron's direction of flight, t is time, Σ_t is the total macroscopic nuclear cross-section, Σ_s is the double differential macroscopic scattering cross-section, and Q is the fixed neutron source. Appropriate initial (4) and boundary (5) conditions that correspond to MagLIF experiments are

$$\psi\left(\vec{r},E,\vec{\Omega},0\right)=0,\quad \vec{r}\in V\quad 0<E<\infty,\quad \vec{\Omega}\in 4\pi, \quad (4)$$

$$\psi\left(\vec{r},E,\vec{\Omega},t\right)=0,\quad \vec{r}\in\partial V\quad 0<E<\infty,\quad \vec{\Omega}\cdot\vec{n}<0,\quad t>0. \quad (5)$$

These conditions reflect the assumption that there are no free streaming neutrons in the system prior to $t=0$, and no neutrons are streaming into the system from the outside.

The solution of the neutron transport equation (3) for source-driven problems can be separated into nth collided fluxes [22, 23]:

$$\psi\left(\vec{r},E,\vec{\Omega},t\right)=\sum_{n=0}^{\infty}\psi_n\left(\vec{r},E,\vec{\Omega},t\right). \quad (6)$$

Physically, $\psi_n\left(\vec{r},E,\vec{\Omega},t\right)$ is the flux due to neutrons that have scattered n times in the system.

The first two terms of series (6) correspond to the primary DD peak and single scattering in the beryllium liner respectively. They will be used to approximate the neutron flux at the front LOS 270 detector for any given MagLIF experiment, i.e.,

$$\psi\left(\vec{r}, E, \vec{\Omega}, t\right) \approx \psi_0\left(\vec{r}, E, \vec{\Omega}, t\right) + \psi_1\left(\vec{r}, E, \vec{\Omega}, t\right). \tag{7}$$

This assumption is consistent with similar techniques found in literature [18, 24, 25, 26, 27]. Integral equations can be written for these quantities [22, 23]

$$\psi_0\left(\vec{r}, E, \vec{\Omega}, t\right) = \int_0^\infty Q\left(\vec{r} - s'\vec{\Omega}, E, \vec{\Omega}, t - \frac{s'}{v}\right) \exp\left(-\int_0^{s'} \Sigma_t\left(\vec{r} - s''\vec{\Omega}, E\right) ds''\right) ds' \tag{8}$$

$$\begin{aligned}\psi_1\left(\vec{r}, E, \vec{\Omega}, t\right) = \int_0^\infty \Bigg[\int_0^\infty dE' \int_{4\pi} d\vec{\Omega}'\ \Sigma_s\left(\vec{r} - s'\vec{\Omega}, E' \to E, \vec{\Omega}' \to \vec{\Omega}\right) \\ \times \psi_0\left(\vec{r} - s'\vec{\Omega}, E', \vec{\Omega}', t - \frac{s'}{v}\right)\Bigg] \exp\left(-\int_0^{s'} \Sigma_t\left(\vec{r} - s''\vec{\Omega}, E\right) ds''\right) ds'\end{aligned} \tag{9}$$

These will be used to inform the time-of-flight expressions for the un-collided and once-collided neutrons in a MagLIF experiment.

IV.A.2. The Neutron Time-of-Flight Solution Technique

The time it takes for a neutron to traverse a distance d is directly related to its kinetic energy:

$$E(t) = m_n\left(\gamma - 1\right) \tag{10}$$

where m_n is the neutron's mass, $\gamma = 1/\sqrt{1-\beta^2}$, $\beta = t_\gamma/t$, $t_\gamma = d/c$, and c is the speed of light. A pulsed beam of poly-energetic neutrons originating at the same point in space and time will arrive a distance d away in some finite time interval. If the energy spectrum of this neutron population is known, then its distribution in time is determined by substituting (10) into the energy spectrum and multiplying by the Jacobian

$$\left|\frac{dE}{dt}\right| = \frac{m_n\gamma^3\beta^3}{t_\gamma}. \tag{11}$$

This is essentially the neutron time-of-flight solution technique, and it is used to transform the energy spectrum of un-collided and once-collided neutrons from a MagLIF experiment into the corresponding time-domain.

If the MagLIF plasma is considered to be an isotropic point source of neutrons with a Gaussian energy spectrum $I(E)$ and burn history $T(t)$, then the problem with a modified source

$$Q\left(\vec{r}, E, \vec{\Omega}, t\right) = \frac{\delta\left(\vec{r}\right) I(E)\delta(t)}{4\pi} \tag{12}$$

can be solved, and the burn history can be convolved with the resulting neutron spectrum to obtain the same solution as the problem with complete source description. It follows, by looking at (8), that for such a source the un-collided neutron spectrum at a point detector situated at $\vec{r}_d$ is given by

$$N_0(E) = A_0 \cdot I(E) \cdot \exp\left(-\Sigma_t(E)(R_o - R_i)\csc\theta\right) \cdot \exp\left(-\sum_{i=1}^{N} \Sigma_{t,i}(E)\Delta x_i\right) \tag{13}$$

where A_0 is a scaling factor, Σ_t is the total macroscopic cross-section of the liner, R_i is the inner radius of the liner, R_o is the outer radius of the liner, θ is the polar angle associated with the neutron direction, N is the number of regions that the neutrons pass through in LOS 270 before arriving at the detector, $\Sigma_{t,i}$ is the total macroscopic cross-section of each of those regions, and Δx_i is the thickness of each region. The cylindrical geometry of the liner is reflected in the first attenuation term of this expression.

The primary scattering region of interest in the proposed neutron spectrum model is the dense beryllium liner. Equation (9) was used as a template to infer an expression for the distribution of once-collided neutrons emanating from this region and heading toward the same point detector:

$$N_1(E) = A_1 \cdot \left\{ \int_0^\infty \int_{4\pi} I(E') \frac{1}{\Sigma_t(E')} \left[1 - \exp\left(-\Sigma_t(E')(R_o - R_i)\csc\theta\right)\right] \right.$$
$$\left. \Sigma_s\left(\vec{r}, E' \rightarrow E, \mu_0\right) d\vec{\Omega}' dE' \right\} \exp\left(-\sum_{i=1}^{N} \Sigma_{t,i}(E)\Delta x_i\right) \tag{14}$$

where A_1 is another scaling factor. In practice, the bounds of the angular integration are defined in terms of the height of the cylindrical liner, H, as well as the radii of the liner, R_i and R_o. The

double differential scattering cross-section can be decomposed into two factors [21]

$$\Sigma_s\left(\vec{r}, E' \rightarrow E, \mu_0\right) = \Sigma_s(\vec{r}, E') p\left(\vec{r}, E' \rightarrow E, \mu_0\right) \tag{15}$$

where $\Sigma_s(\vec{r}, E')$ is the macroscopic scattering cross-section and $p\left(\vec{r}, E' \rightarrow E, \mu_0\right) dE d\vec{\Omega}$ is the probability that a neutron scattering with initial energy E' and direction $\vec{\Omega}'$ will emerge with a new energy E in the interval E to $E + dE$ and new direction $\vec{\Omega}$ in the interval $\vec{\Omega}$ to $\vec{\Omega} + d\vec{\Omega}$. This expression can be decomposed even further to reflect the physics of an elastic scattering event [22]

$$\Sigma_s\left(\vec{r}, E' \rightarrow E, \mu_0\right) = \Sigma_s(\vec{r}, E') p\left(\vec{r}, E' \rightarrow E\right) \delta\left(\mu_0 - f(E', E)\right) \tag{16}$$

where $p\left(\vec{r}, E' \rightarrow E\right) dE$ is the probability that a neutron scattering with initial energy E' will emerge with a new energy E in the interval E to $E + dE$ and $f(E', E)$ is the usual relationship which describes the scattering angle in terms of incoming and outgoing neutron energy. Using a Legendre expansion of the scattering kernel, the once-collided neutron variance can be written explicitly as

$$\begin{aligned} N_1(E) = A_1 \cdot \Bigg\{ \int_0^\infty \int_{4\pi} I(E') \frac{\Sigma_s(E')}{\Sigma_t(E')} \left[1 - \exp\left(-\Sigma_t(E')(R_o - R_i)\csc\theta\right)\right] \\ \left[\frac{1}{(1-\alpha)E'} \sum_{n=0}^{\infty} \frac{2n+1}{2\pi} a_n(E') P_n\left[1 - \frac{(A+1)^2}{2A}\left(1 - \frac{E}{E'}\right)\right]\right] \\ \left[\sum_{l=0}^{\infty} \frac{2l+1}{4\pi} P_l(\mu_0) P_l\left(\frac{A+1}{2}\sqrt{\frac{E}{E'}} - \frac{A-1}{2}\sqrt{\frac{E'}{E}}\right)\right] d\vec{\Omega}' dE' \Bigg\} \\ \exp\left(-\sum_{i=1}^{N} \Sigma_{t,i}(E) \Delta x_i\right) \end{aligned} \tag{17}$$

where $a_n(E')$ are the Legendre moments of the differential scattering cross-section given by ENDF [20], P_n are Legendre polynomials, $\alpha = [(A-1)/(A+1)]^2$, and A is the target nucleus-to-neutron mass ratio.

The analytic model of the once-collided neutron spectrum is completely determined by defining an appropriate expression for the scattering cosine. Notice that by simple vector addition the detector location $\vec{r}_d$ can be expressed in terms of the scattering location $\vec{r}_s(\vec{\Omega}')$ and the direction-

of-flight from the scattering location to the point detector $\vec{r}_{s\to d}(\vec{\Omega})$

$$\vec{r}_d = \vec{r}_s + \vec{r}_{s\to d}. \tag{18}$$

Hence, the cosine of the scattering angle μ_0 is uniquely determined by $\vec{r}_s(\vec{\Omega}')$ and $\vec{r}_d$

$$\mu_0 = \frac{\vec{r}_s \cdot \vec{r}_{s\to d}}{|\vec{r}_s|\,|\vec{r}_{s\to d}|} = \frac{\vec{r}_s \cdot (\vec{r}_d - \vec{r}_s)}{|\vec{r}_s|\,|\vec{r}_d - \vec{r}_s|}. \tag{19}$$

Thus, the full neutron spectrum is finally calculated by adding (13) and (17), substituting (10) in for the energy term, and multiply by the Jacobian (11):

$$N(t - t_0) = [N_0(E(t - t_0)) + N_1(E(t - t_0))] \left|\frac{dE}{dt}\right|. \tag{20}$$

Here t_0 is an arbitrary time shift used to fit the synthetic signal to experimental MagLIF data.

Since there is a distance of 9.5 meters between the detector and source (including the liner) they both look like points to each other. Thus, it is not unreasonable to assume that un-collided and once-collided neutrons emanate from the liner like delta functions in space and time. This is the key assumption that allows a relatively simple expression to be written for the neutron variance. However, the trade-off for an expression of this form is the exclusion of certain physical events. These include neglecting attenuation of back-scattered neutrons through the liner and computing scattering cosines at the liner's edge instead of intermediate positions. The latter assumption will not impact the solution, because a nToF measurement cannot resolve the difference between scattering events in such a small distance. The former assumption can be remedied by excluding the back-scatter region from the fit to data.

IV.A.3. Beamline Attenuation

The attenuation term in the analytic expression of the neutron spectrum was considered for materials in the direct line-of-sight of the point-source to point-detector in LOS 270. Five regions were identified to be the most significant contributors to neutron attenuation. They are identified in Table I ordered from source to detector with their associated material properties and approximate thickness.

TABLE I
There are five significant attenuation regions in LOS 270.

Region	Material	Density	Thickness
Vacuum Window	Stainless Steel 304	8.03 g/cc	0.5 cm
Viewport	Plate Glass	2.40 g/cc	0.5 cm
Mid-point Shield	Tungsten	19.3 g/cc	2.5 cm
Small Front Shield	Tungsten	19.3 g/cc	2.5 cm
Detector Front Plate	Aluminum	2.70 g/cc	0.5 cm

Since the combined thickness and density of both tungsten regions is greater than the other regions, they will contribute the most to attenuation. The tungsten in both regions is a combination of multiple isotopes in various atom percents. Neutrons in the energy range 1-3 MeV will pass through the un-resolved resonance regions of the tungsten isotopes [20]. Hence, attenuation of un-collided or once-collided MagLIF neutrons does not add significant structure to the signal, instead, it uniformly lowers the amplitude of the signal across the energy region of interest.

The other attenuation regions are not as thick or as dense as the tungsten regions, and DD neutrons will pass through their un-resolved resonance regions as well. Thus, it is reasonable to assume that the total beamline attenuation will not significantly change the shape or add unwanted structure to the nToF signal. Therefore, the forward model that was fit to experimental data only includes a tungsten attenuation region. Beamline attenuation would have to be given much more consideration if the total neutron yield were to be extracted from the measured nToF signal. The reason for this is that the height of the nToF and area under its curve are related to the neutron yield. Since this work makes no attempt to infer the total neutron yield, attenuation due to other components in the LOS was disregarded.

IV.B. The Neutron-Burn Time History

The neutron-burn time history is characterized by a burn-width w and bang-time b, which correspond to the FWHM of the neutron-burn time history and the stagnation point respectively [28, 29]. Since the DD and DT fusion reactions are the source of neutrons in a MagLIF experiment, the time history of thermonuclear neutron production can be directly related to the confinement time of the plasma. A sufficiently long plasma confinement time is important for achieving energy

break-even in inertial confinement fusion experiments. Hence, extracting the neutron burn-width from a nToF measurement is relevant for characterizing a MagLIF experiment. A Gaussian distribution was assumed according to the equation

$$T(t) = A \cdot \exp\left(\frac{-4\ln 2(t-b)^2}{w^2}\right) \tag{21}$$

where A is a scaling factor.

IV.C. The Instrument Response Function

The instrument response function is the mapping between the incoming neutron flux and the detected events [30, 31]. Plastic scintillators have a response which consists of a very short rise time followed by a relatively slow exponential decay or sum of decays [32]. Traditionally, effects due to the photomultiplier tube, finite flight path along the scintillator thickness, and the bandwidth of the cabling system and recording instrument are approximated as a Gaussian [32]. By assuming that the response function is the convolution of this Gaussian and a sum of exponential decays, the IRF can be written as a nonlinear function of multiple unknown parameters [32, 33]:

$$R(t) = Q\sum_{i=1}^{N}\frac{f_i}{2\tau_i}\exp\left(-\frac{t-\mu}{\tau_i}\right)\exp\left(\frac{\sigma^2}{2\tau_i^2}\right)\left[1+\operatorname{erf}\left(\frac{t-\mu-\frac{\sigma^2}{\tau_i}}{\sqrt{2\sigma^2}}\right)\right] \tag{22}$$

where Q is the area and total charge extracted (proportional to the energy deposited), f_i is the fraction of the total area corresponding to the particular decay component, μ is the centroid location, σ is the Gaussian width parameter, and τ_i is the scintillator decay parameter. This function is convolved with the time integrated neutron spectrum to produce a synthetic nToF measurement.

Extensive work has gone into measuring the instrument response functions for detectors that are fielded on the Z machine [33]. In the most recent effort, thousands of waveforms were obtained for single DT neutron interactions, and average distributions were calculated. A nonlinear least-squares fitting routine was used to fit (22) to the average waveform, and the parameters were determined as a function of different bias settings. The results of this effort have been meticulously recorded and are used in this work to incorporate the detector response into the neutron time-of-flight signal. This approach assumes equivalency between DT and DD neutron induced IRFs.

Hence, scintillator intensity is implicitly assumed to be independent of the incident neutron energy. See the literature [33] for more details.

V. RESULTS

V.A. Convergence of the Scattering Kernel

The once-collided neutron spectrum is expressed as two infinite series; one that corresponds to the expansion of the differential scattering cross-section and another to the Legendre expansion of the delta function. The angular distribution of elastically scattered neutrons in the energy range 1-3 MeV can be represented by a fourth order Legendre polynomial [20]. Hence, the infinite series representation of the differential scattering cross-section can be truncated after the fifth term. To see where the infinite series representation of the delta function can be reasonably truncated at, the once-collided neutron spectrum was calculated for Legendre polynomials ranging from zero to four degrees. It was found that the once-collided neutron spectrum is approximately converged with five terms, and the delta function can be reasonably approximated in terms of a fourth order Legendre polynomial. Inclusion of higher degree Legendre polynomials increases the computational cost of this method without a noticeable improvement in the model's fidelity. The limitations of Legendre expansion are detailed in literature [34].

V.B. Comparison to Monte Carlo Simulations

The transit time of DD neutrons in the liner is ∼5 ps. Hence, the time it takes for a neutron to reach the scattering location in the liner was neglected. Similarly, the distances of travel from the scattering locations to the detector are all assumed to be equal (in this analysis that distance is 950 cm). The combination plasma and liner is treated as an isotropic point source, and the detector is also thought of as a point. These assumptions are reasonable because of the great contrast in distances from the source to scattering region and source/scattering region to the detector.

There are at least ten parameters that control the shape of the nToF signal to various extents, and they can all be treated as fitting coefficients in the analysis. To preempt the obvious result of returning insensitive coefficient values, five of these parameters are preset at reasonable values that are representative of an average MagLIF experiment. Lists of the unknown and preset parameters of the model are presented in Tables II and III respectively.

TABLE II
The analytic model is characterized by five unknown fitting parameters.

Description	Ion Temperature	Liner Density	Un-collided Scaling	Once-collided Scaling	Time Shift
Symbol	T_i	ρ	A_0	A_1	t_0

TABLE III
Five parameters of the model were preset.

Description	Bang Time	Burn Width	Inner Radius	Outer Radius	Height
Symbol	b	w	R_i	R_o	H
Value	0 ns	2 ns	0.010 cm	0.025 cm	1.0 cm

The approximate neutron spectrum was written in a Matlab script, and numerical results were calculated for a representative MagLIF problem. In this case, the plasma was treated as a single temperature point source situated in the axial/radial center of a hollow beryllium cylinder with dimensions and material properties specified in Table IV.

TABLE IV
MagLIF problem specification for comparison to Monte Carlo simulations.

Ion Temperature	Liner Density	Height	Inner Radius	Outer Radius
2.0 keV	70 g/cc	1.0 cm	0.010 cm	0.025 cm

The same problem was solved using the neutron transport code MCNP [35], except a uniformly distributed line source was used instead of a point source. The reason for this alteration was to see the effects of approximating the plasma as a point source instead of the more realistic line source. The resulting un-collided and once-collided neutron spectrums are plotted in Figures 2 and 3, respectively.

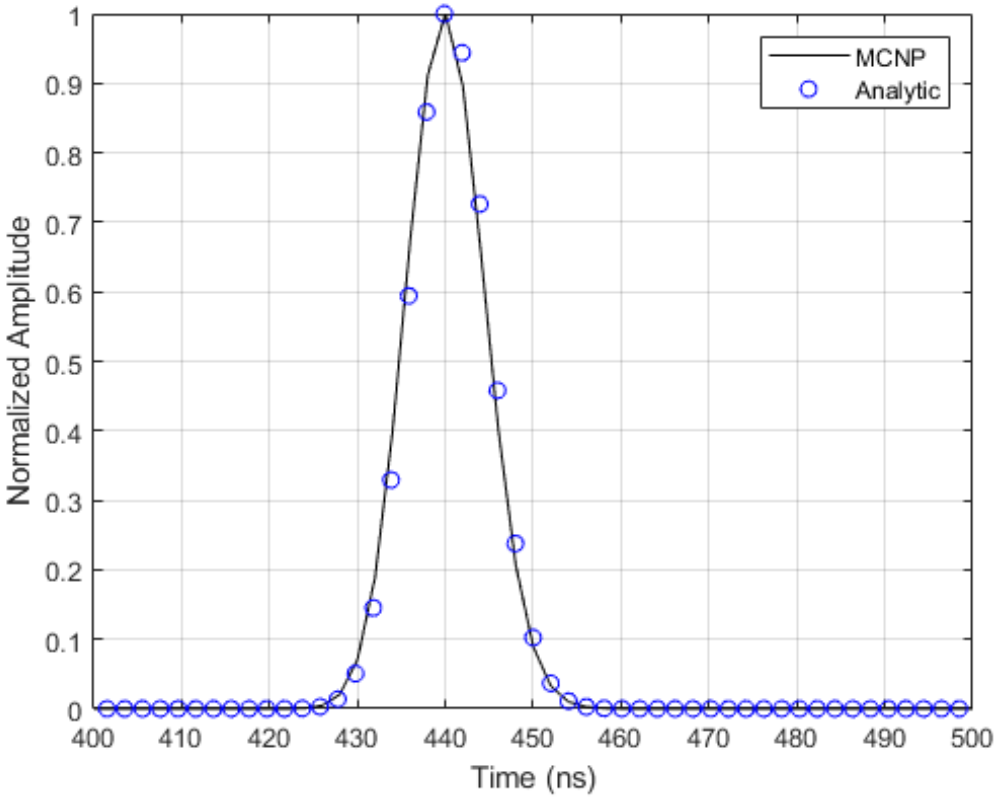

Fig. 2. The un-collided neutron spectrum compared to MC simulations.

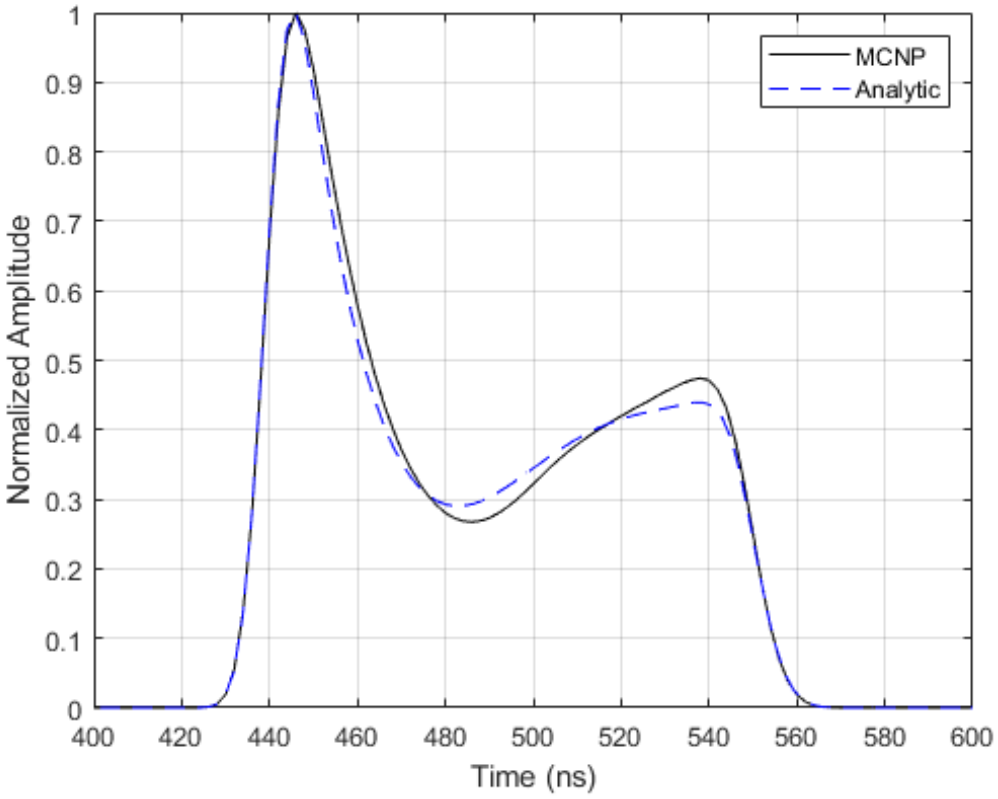

Fig. 3. The once-collided neutron spectrum compared to MC simulations.

There is very good agreement between the analytic and MC representations of the un-collided neutron spectrum. Similarly, there is good agreement between the forward scattered neutrons in the analytic and MC representations of the once-collided neutron spectrum. However, there are some slight discrepancies between the results in the back-scatter region. The reason for this is that the MC simulation takes into account all types of nuclear reactions, not just elastic scattering. These non-elastic events are primarily inelastic scattering and (n,2n) reactions. This would account for the small discrepancies in the curves. It should also be noted that the analytic model does not include attenuation of back-scattered neutrons through the liner. While not drastically changing the shape of the curve, attenuation through the liner would slightly lower the height of the second peak. Similarly, premature truncation of the Legendre polynomial series obfuscates the credibility of the elastic scattering physics model. However, the ion temperature impacts the primary DD peak and the forward scatter peak more than any other part of the signal. Hence, only the primary

and forward scatter peak was used to fit experimental data.

The fitting routine was executed nine times for various initial ion temperature and liner density starting points. In this instance, the initial ion temperatures and liner densities were $T_i \in [1, 2, 3]$ keV and $\rho \in [60, 70, 80]$ g/cc respectively. It was found that the model accurately recovered the input ion temperatures from the synthetic data generated by the MC simulation for all input guess values. This means that the model can confidently recover the true ion temperature of the implosion and is insensitive to the initial guess parameters used in the fit. In contrast, results indicate that the true areal density cannot be inferred using this model as the value inferred by the fit is entirely determined by the guess value used. However, the coefficient of determination for each execution of the fitting algorithm was $R^2 \geq 0.99$. This means that the model can accurately predict the shape of the nToF signal, but the liner density is correlated to one or more of the other model parameters. Figure 9 shows the weak negative correlation between the liner density and the single scatter scaling factor for these MC simulations.

V.C. Comparison to Experimental Data

In this work 20 MagLIF data-sets were analyzed, each one corresponding to a different "shot" or experiment. Only the front LOS 270 detector was considered. Shot 2979 is used as a graphical example of the method. The DD portion of the signal corresponding to shot 2979 is displayed in Figures 4 and 5. This experimental MagLIF data has a well defined primary un-scattered neutron peak and a clear down-scatter region. The average data-set in the shot series that was analyzed has the same basic structure and shape as this representative nToF signal.

A model of the nToF signal with and without single elastic scattering in the beryllium liner was fit to the data and the unknown parameters were extracted. As was mentioned previously, some of the experimental data was excluded from the fit in order to encourage numerical convergence of the fitting routine with respect to the ion temperature. Figure 4 and Table V show the results of fitting the model without scattering. Figure 5 and Table VI show the results of fitting the model with single scatter addition. The coefficients of determination are $\mathrm{R}^2 = 0.9990$ and $\mathrm{R}^2 = 0.9992$, respectively.

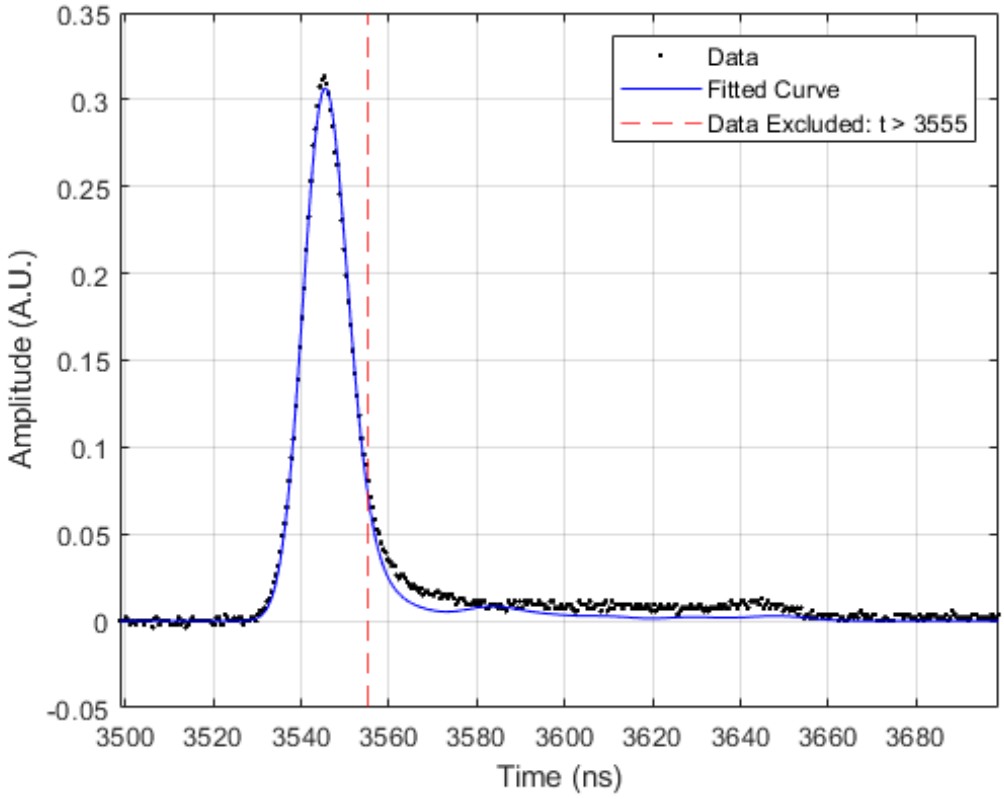

Fig. 4. A model of the nToF signal without scattering was fit to experimental data.

TABLE V
Inferred parameters of the model without scattering.

Parameter	Value	95% CB
T_i	2.052 keV	(1.972, 2.133)
ρ	55.71 g/cc	(-5905, 6016)
A_0	0.00724	(-0.09832, 0.1128)
t_0	3084 ns	(3080, 3088)

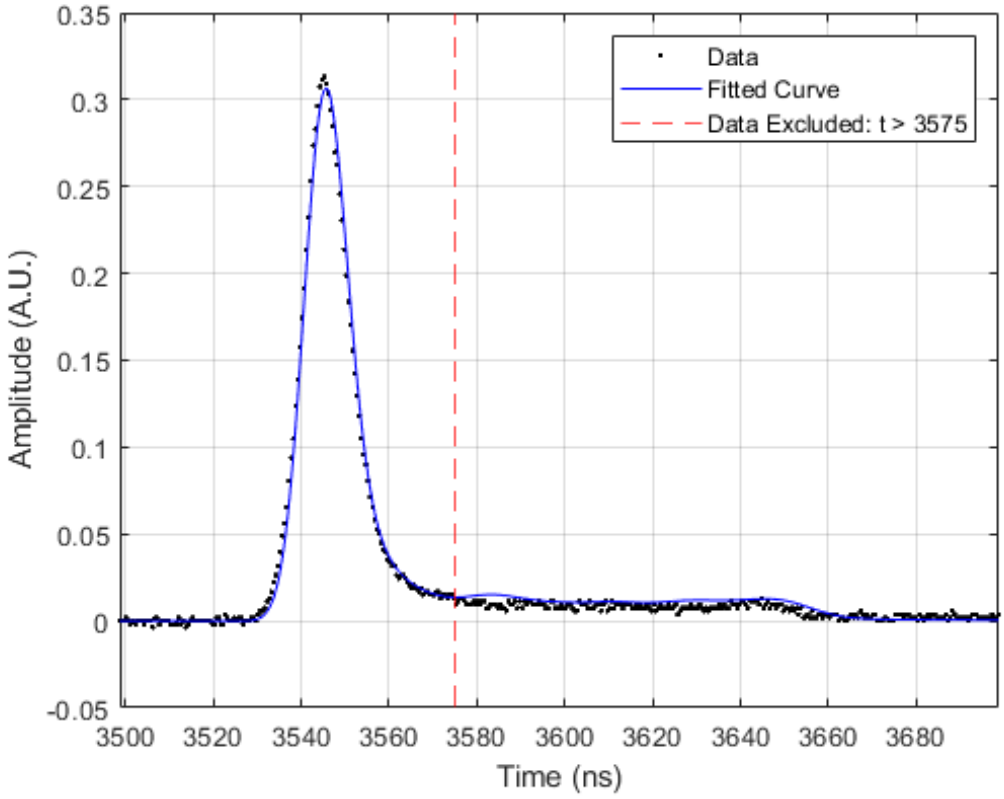

Fig. 5. A model of the nToF signal with single elastic scattering was fit to experimental data.

TABLE VI
Inferred parameters of the model with single elastic scattering.

Parameter	Value	95% CB
T_i	1.911 keV	(1.876, 1.946)
ρ	75.76 g/cc	(-239, 390.6)
A_0	0.007305	(0.001741, 0.01287)
A_1	7.862	(-26.72, 42.44)
t_0	3084 ns	(3083, 3084)

It is clear that both models are only mutually sensitive to the apparent ion temperature and time shift. Since the ion temperature is the more important physical parameter of the two, only it will be reported for the rest of the shots in the series. Figure 6 compares the inferred

ion temperatures from the model without scattering to results that were obtained separately from a simple Gaussian model. The root-mean-square error between the two methods was found to be 0.2254. Figure 7 compares the inferred ion temperatures from the model with single elastic scattering to results that were also obtained separately from high fidelity MC simulations of the Z machine. The root-mean-square error between the two methods was found to be 0.0887. This particular method had the advantage of using a full MC model of the Z machine but suffered the unfortunate drawback of needing to run multiple expensive simulations at various experimental conditions until convergence of the model parameters was found.

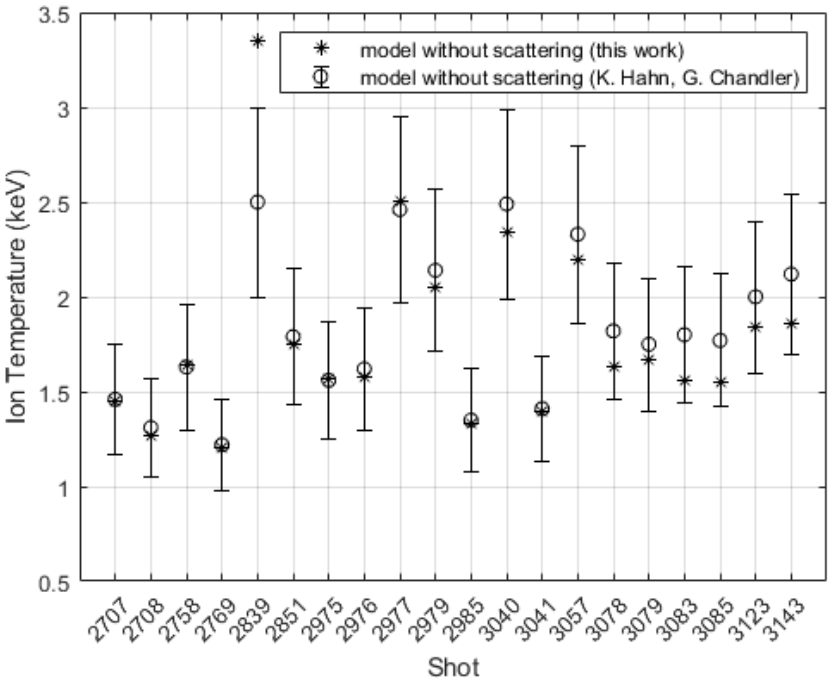

Fig. 6. Comparison of inferred ion temperatures from models without scattering.

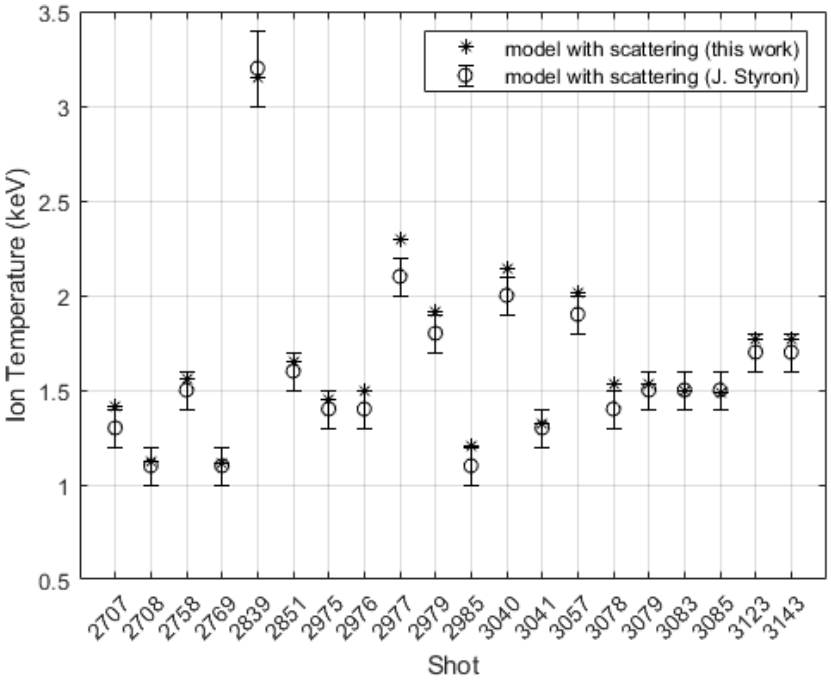

Fig. 7. Comparison of inferred ion temperatures from models with scattering.

It is important to note that this analysis reveals an interesting trend between ion temperatures inferred from models with and without scattering. Figure 8 illustrates this trend. It is clear from this plot that inclusion of scattering consistently lowers the inferred apparent ion temperature. This result is significant because it demonstrates how over-simplification of physics models can lead to over-estimation of important experimental metrics.

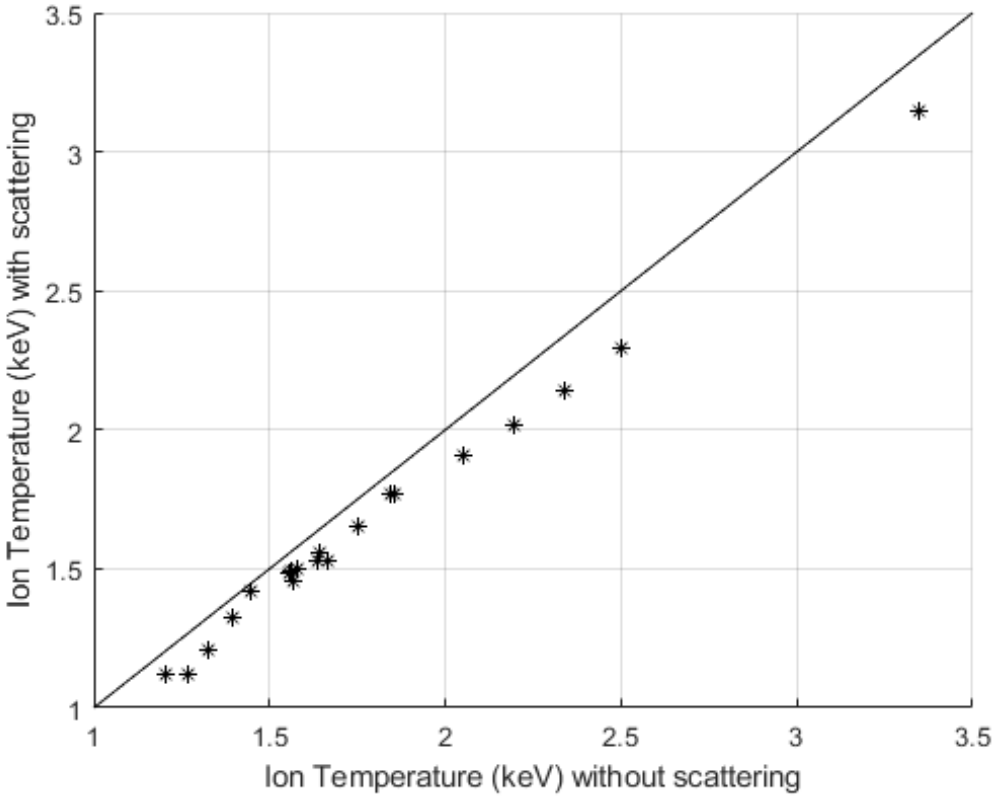

Fig. 8. Including scattering in the model lowers the inferred ion temperature.

Finally, the correlation between the liner density and single scatter scaling factor was investigated. Figure 9 demonstrates a weak negative correlation between these two parameters. This is indicated by the negatively sloped linear trendline and small coefficient of determination. When the liner density is predicted to be small the signal needs to be scaled up and A_1 compensates by being large and vice versa. This means that the shape of the beryllium liner downscatter region is insensitive to the liner density, given this modeling technique.

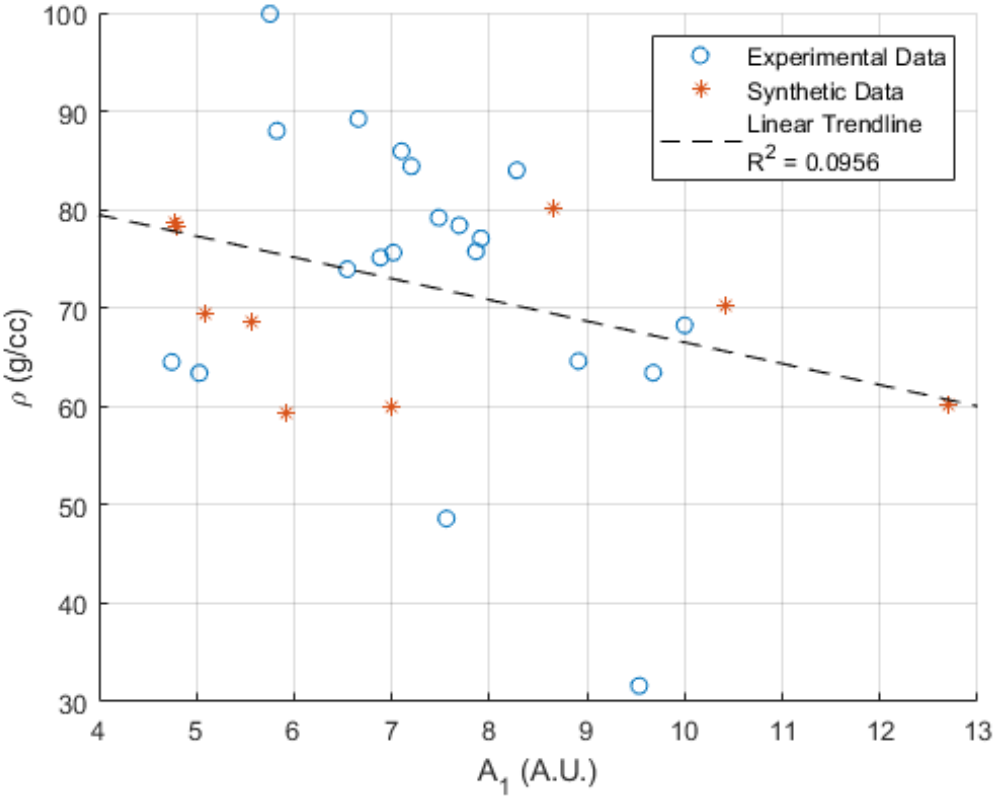

Fig. 9. The liner density and single scatter scaling factor are weakly correlated.

In fact, the liner density behaves as a scaling factor itself. Hence, having both ρ and A_1 in the model is essentially equivalent to having two scaling factors that serve the same purpose. However, both are needed to guarantee that the experimental data can accurately be reproduced. This oddity demands that A_1 should be eliminated from the model so that the liner density can be predicted more accurately. To do this, an expression relating ρ and A_1 must be determined. Since these parameters are only weakly correlated, an expression such as this could not easily be produced by running MC simulations, fitting the model to resulting synthetic data, and developing correlations. Thus, an analytical expression must be determined. Degeneracy can be removed by constructing a downscatter-ratio type relationship, but this method still relies on simplified analytic transport expressions for the un-collided and once-collided neutron spectra. These problems can be overcome using a more sophisticated approach, which is presented in the future work section.

VI. DISCUSSION

The model without scattering is not sensitive to the liner density and the scaling parameter of the un-collided neutron spectrum. This is evident from the relatively large widths of the 95% confidence intervals in Table V. The model with single elastic scattering is more sensitive to the scaling parameter of the un-collided neutron spectrum and just slightly more sensitive to the liner density, although the confidence interval is still fairly large for this parameter. Similarly, the results are not sensitive to the scaling parameter of the once-collided neutron spectrum as seen in Table VI. Both of the models are undeniably sensitive to the ion temperature and time shift. Although the sensitivity of the model to the liner density is improved by including single elastic scattering, it is not improved enough to confidently report accurate values of the liner areal density. This particular shortcoming of this method is due to the degeneracy of the liner density and the single elastic scattering scaling factor.

Comparison of inferred ion temperatures to results from previously established techniques proves the validity of this method. The model without scattering compares well with known ion temperatures from a similar method. In most cases the results are either identical after rounding or slightly smaller than the reported values. Discrepancies in the ion temperatures may come from multiple sources. The main culprits are most likely differences in the data excluded from the fit, representation of the neutron energy spectrum, e.g., Brysk versus Ballabio, variation in the neutron-burn time history, and differing instrument response functions.

Ion temperatures inferred from the model with single elastic scattering compare well with those that were inferred from the forward fitting MC simulation technique. Indeed, when the values are not identically equal after rounding they only differ by 0.1 keV on average. The high fidelity MC model of MagLIF experiments on the Z machine is presumably the most accurate way to obtain ion temperatures. Hence, agreement to such a close degree indicates that the accuracy of ion temperatures inferred from nToF signals is dominated by elastic scattering in the beryllium liner. Therefore, it is prudent to at least include single liner scattering in a forward fitting analytic model when high fidelity transport simulations are unavailable or too costly to perform.

VII. SUMMARY AND FUTURE WORK

The goal of this work was to demonstrate how an analytic model of MagLIF nToF signals with single elastic scattering in the liner and beamline attenuation could be used to extract plasma parameters from measured data. It was found that artificial scaling parameters were necessary to fit the model to data but also created degeneracy with the liner density. The ion temperature can be successfully extracted using the method presented in this work, but inferred values change as more physically accurate transport models are employed. Similarly, many assumptions about how neutrons were allowed to behave in the system needed to be specified in order to make the problem tractable. This is the primary shortcoming of this method and others like it. Improving this analysis or coupling it with other physical events, such as time-dependent nuclear cross-sections, plasma-physics simulations, charged particle interactions, or photon transport, is only possible when a complete description of the physics is sacrificed. Thus, a better approach is needed.

It is possible to use a full physics transport simulation to calculate sensitivity coefficients of nToF signals and other experimental neutron measurements with respect to model parameters. These relative derivatives can be used in conjunction with a generalized linear-least-squares methodology to adjust guessed parameter values and calibrate detector signals. Consistent with a Bayesian inference formalism, this technique can be used to infer experimental parameters from data and reduce uncertainty in estimated values. Artificial scaling parameters and other quantities like them are not needed in an approach such as this. More importantly, this technique will allow a multi-physics analysis of these systems to be explored via a chain rule expansion of the sensitivity coefficients in question. Hence, future work will be focused on a modular approach to determining sensitivity coefficients of separate physical systems and then coupling them together in a comprehensive suite of experimental diagnostic analysis techniques.

ACKNOWLEDGMENTS

Kelly Hahn and Carlos Ruiz were influential in the early stages of this work.

Sandia National Laboratories is a multimission laboratory managed and operated by National Technology & Engineering Solutions of Sandia, LLC, a wholly owned subsidiary of Honeywell International Inc., for the U.S. Department of Energy's National Nuclear Security Administration under contract DE-NA0003525. This paper describes objective technical results and analysis. Any subjective views or opinions that might be expressed in the paper do not necessarily represent the views of the U.S. Department of Energy or the United States Government.

REFERENCES

[1] M. E. Savage, L. F. Bennett, D. E. Bliss, W. T. Clark, R. S. Coats, J. M. Elizondo, K. R. LeChien, H. C. Harjes, J. M. Lehr, J. E. Maenchen, D. H. McDaniel, M. F. Pasik, T. D. Pointon, A. C. Owen, D. B. Seidel, D. L. Smith, B. S. Stoltzfus, K. W. Struve, W. A. Stygar, L. K. Warne, J. R. Woodworth, C. W. Mendel, K. R. Prestwich, R. W. Shoup, D. L. Johnson, J. P. Corley, K. C. Hodge, T. C. Wagoner, and P. E. Wakeland, "An overview of pulse compression and power flow in the upgraded Z pulsed power driver," **2**, 979 (2007); 10.1109/PPPS.2007.4652354.

[2] D. V. Rose, D. R. Welch, E. A. Madrid, C. L. Miller, R. E. Clark, W. A. Stygar, M. E. Savage, G. A. Rochau, J. E. Bailey, T. J. Nash, M. E. Sceiford, K. W. Struve, P. A. Corcoran, and B. A. Whitney, "Three-dimensional electromagnetic model of the pulsed-power Z-pinch accelerator," *Phys. Rev. ST Accel. Beams*, **13**, 010402 (2010); 10.1103/PhysRevSTAB.13.010402., URL https://link.aps.org/doi/10.1103/PhysRevSTAB.13.010402.

[3] M. E. Savage, K. R. LeChien, M. R. Lopez, B. S. Stoltzfus, W. A. Stygar, D. S. Artery, J. A. Lott, and P. A. Corcoran, "Status of the Z pulsed power driver," 983–990 (2011); 10.1109/PPC.2011.6191629.

[4] R. B. Spielman, C. Deeney, M. R. Douglas, G. A. Chandler, M. E. Cuneo, T. J. Nash, J. L. Porter, L. E. Ruggles, T. W. L. Sanford, W. A. Stygar, K. W. Struve, M. K. Matzen, D. H. McDaniel, D. L. Peterson, and J. H. Hammer, "Wire-array z pinches as intense x-ray sources for inertial confinement fusion," *Plasma Physics and Controlled Fusion*, **42**, *12B*, B157 (2000); 10.1088/0741-3335/42/12b/312., URL https://doi.org/10.1088%2F0741-3335%2F42%2F12b%2F312.

[5] T. W. L. Sanford, R. W. Lemke, R. C. Mock, G. A. Chandler, R. J. Leeper, C. L. Ruiz, D. L. Peterson, R. E. Chrien, G. C. Idzorek, R. G. Watt, and J. P. Chittenden, "Dynamics and characteristics of a 215-eV dynamic-hohlraum x-ray source on Z," *Physics of Plasmas*, **9**, *8*, 3573 (2002); 10.1063/1.1489676., URL https://doi.org/10.1063/1.1489676.

[6] M. C. Jones, D. J. Ampleford, M. E. Cuneo, R. Hohlfelder, C. A. Jennings, D. W. Johnson, B. Jones, M. R. Lopez, J. MacArthur, J. A. Mills, T. Preston, G. A. Rochau, M. Savage, D. Spencer, D. B. Sinars, and J. L. Porter, "X-ray power and yield measurements at the refurbished Z machine," *Review of Scientific Instruments*, **85**, *8*, 083501 (2014); 10.1063/1.4891316., URL https://doi.org/10.1063/1.4891316.

[7] M. E. Cuneo, M. C. Herrmann, D. B. Sinars, S. A. Slutz, W. A. Stygar, R. A. Vesey, A. B. Sefkow, G. A. Rochau, G. A. Chandler, J. E. Bailey, J. L. Porter, R. D. McBride, D. C. Rovang, M. G. Mazarakis, E. P. Yu, D. C. Lamppa, K. J. Peterson, C. Nakhleh, S. B. Hansen, A. J. Lopez, M. E. Savage, C. A. Jennings, M. R. Martin, R. W. Lemke, B. W. Atherton, I. C. Smith, P. K. Rambo, M. Jones, M. R. Lopez, P. J. Christenson, M. A. Sweeney, B. Jones, L. A. McPherson, E. Harding, M. R. Gomez, P. F. Knapp, T. J. Awe, R. J. Leeper, C. L. Ruiz, G. W. Cooper, K. D. Hahn, J. McKenney, A. C. Owen, G. R. McKee, G. T. Leifeste, D. J. Ampleford, E. M. Waisman, A. Harvey-Thompson, R. J. Kaye, M. H. Hess, S. E. Rosenthal, and M. K. Matzen, "Magnetically Driven Implosions for Inertial Confinement Fusion at Sandia National Laboratories," *IEEE Transactions on Plasma Science*, **40**, *12*, 3222 (2012); 10.1109/TPS.2012.2223488.

[8] A. B. Sefkow, S. A. Slutz, J. M. Koning, M. M. Marinak, K. J. Peterson, D. B. Sinars, and R. A. Vesey, "Design of magnetized liner inertial fusion experiments using the Z facility," *Physics of Plasmas*, **21**, *7*, 072711 (2014); 10.1063/1.4890298.

[9] S. A. Slutz, M. C. Herrmann, R. A. Vesey, A. B. Sefkow, D. B. Sinars, D. C. Rovang, K. J. Peterson, and M. E. Cuneo, "Pulsed-power-driven cylindrical liner implosions of laser preheated fuel magnetized with an axial field," *Physics of Plasmas*, **17**, *5*, 056303 (2010); 10.1063/1.3333505.

[10] S. A. Slutz and R. A. Vesey, "High-Gain Magnetized Inertial Fusion," *Phys. Rev. Lett.*, **108**, 025003 (2012); 10.1103/PhysRevLett.108.025003., URL https://link.aps.org/doi/10.1103/PhysRevLett.108.025003.

[11] S. A. Slutz, M. R. Gomez, S. B. Hansen, E. C. Harding, B. T. Hutsel, P. F. Knapp, D. C. Lamppa, T. J. Awe, D. J. Ampleford, D. E. Bliss, G. A. Chandler, M. E.

Cuneo, M. Geissel, M. E. Glinsky, A. J. Harvey-Thompson, M. H. Hess, C. A. Jennings, B. Jones, G. R. Laity, M. R. Martin, K. J. Peterson, J. L. Porter, P. K. Rambo, G. A. Rochau, C. L. Ruiz, M. E. Savage, J. Schwarz, P. F. Schmit, G. Shipley, D. B. Sinars, I. C. Smith, R. A. Vesey, and M. R. Weis, "Enhancing performance of magnetized liner inertial fusion at the Z facility," *Physics of Plasmas*, **25**, *11*, 112706 (2018); 10.1063/1.5054317., URL https://doi.org/10.1063/1.5054317.

[12] M. R. Gomez, S. A. Slutz, A. B. Sefkow, D. B. Sinars, K. D. Hahn, S. B. Hansen, E. C. Harding, P. F. Knapp, P. F. Schmit, C. A. Jennings, T. J. Awe, M. Geissel, D. C. Rovang, G. A. Chandler, G. W. Cooper, M. E. Cuneo, A. J. Harvey-Thompson, M. C. Herrmann, M. H. Hess, O. Johns, D. C. Lamppa, M. R. Martin, R. D. McBride, K. J. Peterson, J. L. Porter, G. K. Robertson, G. A. Rochau, C. L. Ruiz, M. E. Savage, I. C. Smith, W. A. Stygar, and R. A. Vesey, "Experimental Demonstration of Fusion-Relevant Conditions in Magnetized Liner Inertial Fusion," *Phys. Rev. Lett.*, **113**, 155003 (2014); 10.1103/PhysRevLett.113.155003., URL https://link.aps.org/doi/10.1103/PhysRevLett.113.155003.

[13] M. R. Gomez, S. A. Slutz, A. B. Sefkow, K. D. Hahn, S. B. Hansen, P. F. Knapp, P. F. Schmit, C. L. Ruiz, D. B. Sinars, E. C. Harding, C. A. Jennings, T. J. Awe, M. Geissel, D. C. Rovang, I. C. Smith, G. A. Chandler, G. W. Cooper, M. E. Cuneo, A. J. Harvey-Thompson, M. C. Herrmann, M. H. Hess, D. C. Lamppa, M. R. Martin, R. D. McBride, K. J. Peterson, J. L. Porter, G. A. Rochau, M. E. Savage, D. G. Schroen, W. A. Stygar, and R. A. Vesey, "Demonstration of thermonuclear conditions in magnetized liner inertial fusion experiments," *Physics of Plasmas*, **22**, *5*, 056306 (2015); 10.1063/1.4919394., URL https://aip.scitation.org/doi/abs/10.1063/1.4919394.

[14] S. A. Slutz, W. A. Stygar, M. R. Gomez, K. J. Peterson, A. B. Sefkow, D. B. Sinars, R. A. Vesey, E. M. Campbell, and R. Betti, "Scaling magnetized liner inertial fusion on Z and future pulsed-power accelerators," *Physics of Plasmas*, **23**, *2*, 022702 (2016); 10.1063/1.4941100., URL https://doi.org/10.1063/1.4941100.

[15] P. K. Rambo, I. C. Smith, J. L. Porter, M. J. Hurst, C. S. Speas, R. G. Adams, A. J. Garcia, E. Dawson, B. D. Thurston, C. Wakefield, J. W. Kellogg, M. J. Slattery, H. C. Ives, R. S. Broyles, J. A. Caird, A. C. Erlandson, J. E. Murray, W. C. Behrendt, N. D. Neilsen, and J. M. Narduzzi, "Z-Beamlet: a multikilojoule, terawatt-class laser system," *Appl. Opt.*, **44**, *12*, 2421 (2005); 10.1364/AO.44.002421., URL http://ao.osa.org/abstract.cfm?URI=ao-44-12-2421.

[16] L. Ballabio, J. Källne, and G. Gorini, "Relativistic calculation of fusion product spectra for thermonuclear plasmas," *Nuclear Fusion*, **38**, *11*, 1723–1735 (1998); 10.1088/0029-5515/38/11/310.

[17] F. G. Tricomi, *Integral equations F.G. Tricomi*, Interscience Publishers (1957).

[18] R. Hatarik, D. B. Sayre, J. A. Caggiano, T. Phillips, M. J. Eckart, E. J. Bond, C. Cerjan, G. P. Grim, E. P. Hartouni, J. P. Knauer, and et al., "Analysis of the neutron time-of-flight spectra from inertial confinement fusion experiments," *Journal of Applied Physics*, **118**, *18*, 184502 (2015); 10.1063/1.4935455.

[19] Z. L. Mohamed, O. M. Mannion, E. P. Hartouni, J. P. Knauer, and C. J. Forrest, "A generalized forward fit for neutron detectors with energy-dependent response functions," *Journal of Applied Physics*, **128**, *21*, 214501 (2020); 10.1063/5.0033117., URL https://doi.org/10.1063/5.0033117.

[20] D. Brown, M. Chadwick, R. Capote, A. Kahler, A. Trkov, M. Herman, A. Sonzogni, Y. Danon, A. Carlson, M. Dunn, D. Smith, G. Hale, G. Arbanas, R. Arcilla, C. Bates, B. Beck, B. Becker, F. Brown, R. Casperson, J. Conlin, D. Cullen, M.-A. Descalle, R. Firestone, T. Gaines, K. Guber, A. Hawari, J. Holmes, T. Johnson, T. Kawano, B. Kiedrowski, A. Koning, S. Kopecky, L. Leal, J. Lestone, C. Lubitz, J. M. Damián, C. Mattoon, E. McCutchan, S. Mughabghab, P. Navratil, D. Neudecker, G. Nobre, G. Noguere, M. Paris, M. Pigni, A. Plompen, B. Pritychenko, V. Pronyaev, D. Roubtsov, D. Rochman, P. Romano, P. Schillebeeckx, S. Simakov, M. Sin, I. Sirakov, B. Sleaford, V. Sobes, E. Soukhovitskii, I. Stetcu, P. Talou, I. Thompson, S. van der Marck, L. Welser-Sherrill, D. Wiarda,

M. White, J. Wormald, R. Wright, M. Zerkle, G. Žerovnik, and Y. Zhu, "ENDF/B-VIII.0: The 8th Major Release of the Nuclear Reaction Data Library with CIELO-project Cross Sections, New Standards and Thermal Scattering Data," *Nuclear Data Sheets*, **148**, 1 (2018); https://doi.org/10.1016/j.nds.2018.02.001., URL http://www.sciencedirect.com/science/article/pii/S0090375218300206, special Issue on Nuclear Reaction Data.

[21] J. J. Duderstadt and L. J. Hamilton, *Nuclear reactor analysis*, Wiley (1976).

[22] G. I. Bell and S. Glasstone, *Nuclear reactor theory*, R.E. Krieger (1985).

[23] D. G. Cacuci, *Handbook of nuclear engineering*, Springer (2010).

[24] C. J. Forrest, P. B. Radha, V. Y. Glebov, V. N. Goncharov, J. P. Knauer, A. Pruyne, M. Romanofsky, T. C. Sangster, M. J. Shoup, C. Stoeckl, D. T. Casey, M. Gatu-Johnson, and S. Gardner, "High-resolution spectroscopy used to measure inertial confinement fusion neutron spectra on Omega (invited)," *Review of Scientific Instruments*, **83**, *10*, 10D919 (2012); 10.1063/1.4742926., URL https://doi.org/10.1063/1.4742926.

[25] F. Weilacher, P. B. Radha, and C. Forrest, "Three-dimensional modeling of the neutron spectrum to infer plasma conditions in cryogenic inertial confinement fusion implosions," *Physics of Plasmas*, **25**, *4*, 042704 (2018); 10.1063/1.5016856., URL https://doi.org/10.1063/1.5016856.

[26] A. J. Crilly, B. D. Appelbe, K. McGlinchey, C. A. Walsh, J. K. Tong, A. B. Boxall, and J. P. Chittenden, "Synthetic nuclear diagnostics for inferring plasma properties of inertial confinement fusion implosions," *Physics of Plasmas*, **25**, *12*, 122703 (2018); 10.1063/1.5027462., URL https://doi.org/10.1063/1.5027462.

[27] A. J. Crilly, B. D. Appelbe, O. M. Mannion, C. J. Forrest, V. Gopalaswamy, C. A. Walsh, and J. P. Chittenden, "Neutron backscatter edge: A measure of the hydrodynamic properties of the dense DT fuel at stagnation in ICF experiments," *Physics of Plasmas*, **27**, *1*, 012701 (2020); 10.1063/1.5128830., URL https://doi.org/10.1063/1.5128830.

[28] R. A. Lerche, D. R. Kania, S. M. Lane, G. L. Tietbohl, C. K. Bennett, and G. P. Baltzer, "Neutron emission time measurements for ICF targets," *Review of Scientific Instruments*, **59**, *8*, 1697 (1988); 10.1063/1.1140137., URL https://doi.org/10.1063/1.1140137.

[29] R. A. Lerche, D. W. Phillion, and G. L. Tietbohl, "25 ps neutron detector for measuring ICF-target burn history," *Review of Scientific Instruments*, **66**, *1*, 933 (1995); 10.1063/1.1146212., URL https://doi.org/10.1063/1.1146212.

[30] G. F. Knoll, *Radiation detection and measurement / Glenn F. Knoll*, Wiley (2000).

[31] N. Tsoulfanidis and S. Landsberger, *Measurement and detection of radiation*, CRC Press (2015).

[32] T. J. Murphy, R. E. Chrien, and K. A. Klare, "Interpretation of neutron time-of-flight signals from current-mode detectors," *Review of Scientific Instruments*, **68**, *1*, 610 (1997); 10.1063/1.1147763., URL https://doi.org/10.1063/1.1147763.

[33] J. D. Styron, C. L. Ruiz, K. D. Hahn, G. W. Cooper, G. A. Chandler, B. Jones, B. R. McWatters, C. J. Forrest, J. Vaughan, J. Torres, S. Pelka, J. Smith, and C. Weaver, "Average neutron time-of-flight instrument response function inferred from single D-T neutron events within a plastic scintillator," *Review of Scientific Instruments*, **89**, *10*, 10I119 (2018); 10.1063/1.5038883., URL https://doi.org/10.1063/1.5038883.

[34] A. TAKAHASHI, J. YAMAMOTO, M. EBISUYA, and K. SUMITA, "Method for Calculating Anisotropic Neutron Transport Using Scattering Kernel without Polynomial Expansion," *Journal of Nuclear Science and Technology*, **16**, *1*, 1 (1979); 10.1080/18811248.1979.9730865., URL https://doi.org/10.1080/18811248.1979.9730865.

[35] T. Goorley, M. James, T. Booth, F. Brown, J. Bull, L. J. Cox, J. Durkee, J. Elson, M. Fensin, R. A. Forster, J. Hendricks, H. G. Hughes, R. Johns, B. Kiedrowski, R. Martz, S. Mashnik, G. McKinney, D. Pelowitz, R. Prael, J. Sweezy, L. Waters, T. Wilcox, and T. Zukaitis, "Initial MCNP6 Release Overview," *Nuclear Technology*, **180**, *3*, 298 (2012); 10.13182/NT11-135., URL https://doi.org/10.13182/NT11-135.